High-Resolution Imaging Utilizing Space-Frequency DORT Combining the Extrapolated Virtual Array

[1]Qiang Du, [1]Yaoliang Song , [1]Tong Mu, [1]Zeeshan Ahmad
School of electronic and optical engineering, Nanjing University of science and technology, Nanjing, China
E-mails: qdu1023@gmail.com, ylsong@njust.edu.cn, mtonylucky@gmail.com, dr.zeeshan@njust.edu.cn

Abstract—**Space-frequency DORT (SF-DORT) is an effective time-reversal (TR) imaging method due to its immunity to the noise and adaptability of complex environment. However, some potential drawbacks, such as low range and co-range resolutions, make SF-DORT inferior to the Space-frequency MUSIC (SF-MUSIC). In this paper, we propose a novel high-resolution imaging method utilizing SF-DORT combining an extrapolated virtual array (EA-SF-DORT). The virtual extrapolated TR array is created by autoregressive vector extrapolation (ARVE). In this way, the aperture of the TR array is extended significantly and the drawbacks associated with SF-DORT can be improved. Simulation results demonstrate that SF-DORT combining the extrapolated virtual array achieve much higher range and co-range resolutions than conventional SF-DORT.**

Index Terms—Time-reversal (TR) imaging, the decomposition of the time-reversal operator (DORT), Space-frequency DORT (SF-DORT), Extrapolated array, Autoregressive vector extrapolation (ARVE).

I. INTRODUCTION

Time reversal (TR) technique has attracted enormous attention in radar imaging fields in recent years due to its spatial and temporal high-resolution focusing characteristics [1]. The TR operator (TRO) is one of the most fundamental TR imaging method, and TRO form the basis of the decomposition of the time-reversal operator (DORT) and the TR multiple signal classification (TR-MUSIC) [2]-[4]. Space-frequency decomposition of the time-reversal operator (SF-DORT) and SF multiple signal classification (SF-MUSIC) are faster TR imaging methods because they obtain the multistatic data matrices (MDMs) much more conveniently than DORT and TR-MUSIC [5]-[8]. Although SF-DORT works well under increased clutter and noise levels, its range and co-range resolutions are inferior to SF-MUSIC [9].

To overcome the shortcomings of SF-DORT, utilizing virtual extrapolated array is a promising solution because it is suitable for an array with limited aperture and meets the requirement of miniaturizing the imaging system [10]. The autoregressive vector extrapolation (ARVE) [11], which exploits the spatial-temporal coupling of the matrix constituted by the received signals, predicts the signals on the virtual antennas more accurately than the 1-D AR extrapolation in [12]-[13].

Based on the above analysis, we propose a novel high-resolution imaging method utilizing SF-

DORT combining the virtual extrapolated array (EA-SF-DORT) in this article. The performance deterioration of imaging caused by applying the ARVE with the noise matrix can be offset by SF-DORT, and high-resolution can be achieved. Simulations show that SF-DORT utilizing the extrapolated virtual array can achieve much higher range and co-range resolutions than without utilizing.

The rest of this paper is organized as follows. Section II shows the whole processing chain of the proposed TR imaging method, including the principle of ARVE and SF-DORT. To illustrate the high-resolution imaging capability, computer simulations are conducted, and the results are given in Section III. Finally, Section IV offers some conclusions drawn on the basis of simulation results.

II. THE PRINCIPLE OF PROPOSED TR IMAGING METHOD

The processing chain of this novel method is shown in Fig. 1 and could be divided into two stages. In the first stage, the matrix constituted by the received noised-signals, or called the original measurement data set, $\mathbf{S}$, is extrapolated by ARVE. Afterwards, the SF-DORT has been applied to the extrapolated matrix $\mathbf{S}_E$ and high-resolution targets imaging has been achieved.
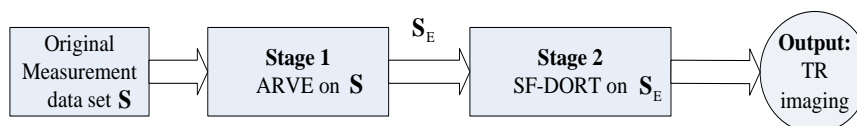

Fig. 1. The processing chain of the new TR imaging method.

A. The principle of ARVE

Assume a TR array, which contains L real antennas, lies parallel to the x-axis. Assume the TR array receives the same linear frequency modulated (LFM) signals, so the received signals are coherent. The received signal on the l-th real antenna is given below

$$s_l(n) = s(l,n) = \left[\sum_{m=1}^{M} s(t - \frac{\rho_{ml}}{c})\right] + n_l(t)\Bigg|_{t=n/f_s} \quad , \tag{1}$$

where ρ_{ml} is the distance from the m-th target to the l-th antenna. m is the target index and $m = 1, 2, \cdots, M$. All the targets are located in the far field. l is the antenna index and $l = 1, 2, \cdots, L$. n is the temporal sampling index and $n = 0, 1, \cdots, N$. f_s is the sampling rate. $n_l(t)$ is the noise on the l-th antenna. $s(t)$ is the LFM signal and can be expressed as follow

$$s(t) = \cos(2\pi(f_0(t) - \frac{1}{2}\mu t^2)) \quad , \tag{2}$$

where $\mu = B / t_0$, B is the signal bandwidth, t_0 is the duration of the signal $t_0 = N/f_s$ and f_0 is the starting frequency. So the centre frequency of the LFM signal is $f_0 - B/2$. Over N measurements, we have the block of time-domain measurement data, denoted by $\mathbf{S}$, of size $L \times N$, as given below

$$\mathbf{S} = \begin{bmatrix} s(1,0) & s(1,1) & \cdots & s(1,N-1) \\ s(2,0) & s(2,1) & \vdots & s(2,N-1) \\ \vdots & \vdots & \ddots & \vdots \\ s(L,0) & s(L,1) & \cdots & s(L,N-1) \end{bmatrix} . \tag{3}$$

With the original measurement data $\mathbf{S}$ in hand, the extrapolated data $\mathbf{S}_E$ is formulated through ARVE.

The principle of ARVE is shown in Fig. 2 and can be divided into three steps.
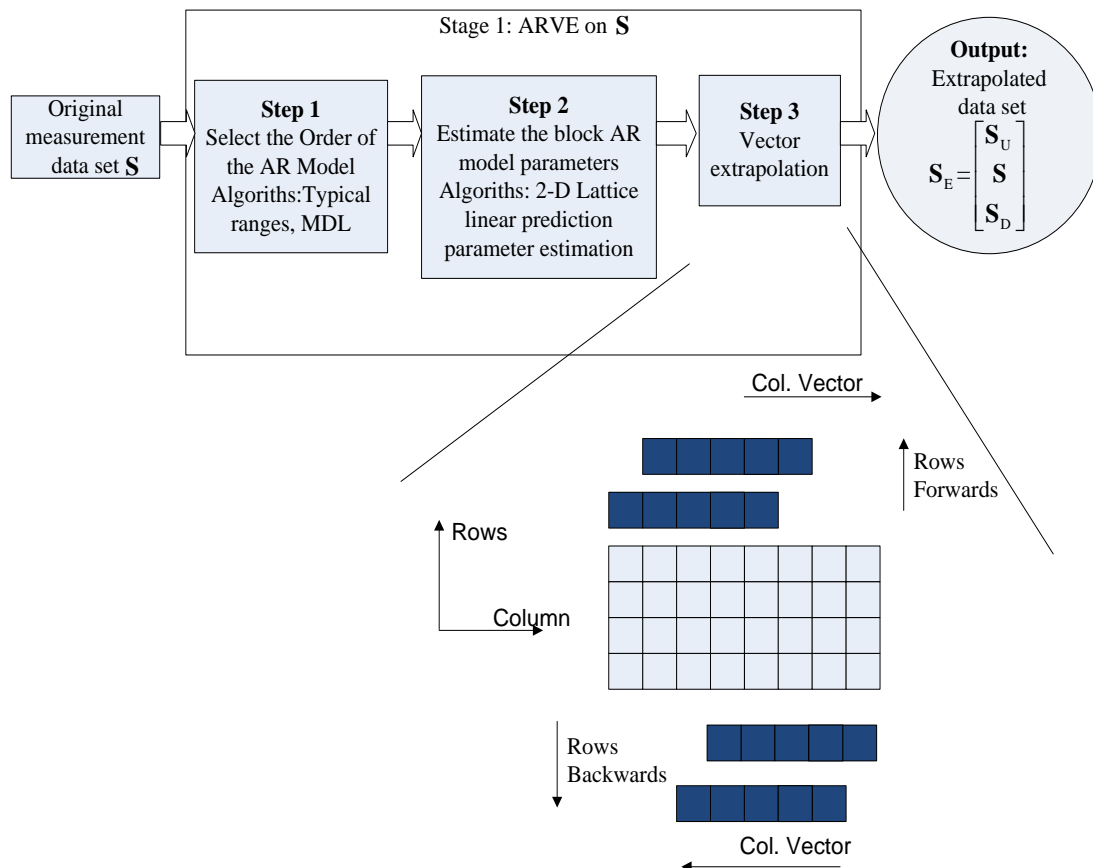

Fig. 2. Virtual measurement data are created by modeling the original measurements with a 2-D AR model and then using vector extrapolation

The first step is to determine the number of parameters of $\mathbf{S}$, i.e. select the order of the AR model. The number of parameters is denoted by a pair (p_1, p_2), where p_1 is the order of the spatial dimension and p_2 is the order of the temporal dimension. Both p_1 and p_2 are positive integers and can be determined by $\mathbf{S}$ itself. This step can be done by choosing the typical value of the model order directly or using an order estimation algorithm such as MDL [14]. The typical range for p_1 is between 1 and $L/2$. The typical range for p_2 is between 1 and $N/2$. The pair (1, 1) should be excluded [10].

With the number of parameters determined, the next step is estimating the block AR model parameters. We will adopt the approach 2-D lattice linear prediction parameter estimation in [15] because it gives a recursive solution for the 2-D AR parameter matrices and it is a fast algorithm.

In the last stage, we provide a brief summary of the vector extrapolation equations. Given a column vector of size $(p_2 + 1) \times 1$ as follows

$$\mathbf{s}_{p_2}(n_1, n_2) = \begin{bmatrix} s(n_1, n_2) & s(n_1, n_2 - 1) & \cdots & s(n_1, n_2 - p_2) \end{bmatrix}^T \quad , \tag{4}$$

and the forward linear vector extrapolation is given in (5)

$$\hat{\mathbf{s}}_{p_2}^F(n_1, n_2) = -\sum_{i=1}^{p_1} \mathbf{A}_{p_2}(i) \mathbf{s}_{p_2}(n_1 - i, n_2) \quad , \tag{5}$$

where $\hat{\mathbf{s}}_{p_2}^F(n_1, n_2)$ is the virtual measurement vector of size $(p_2 + 1) \times 1$, and the superscript F represents forward. $\mathbf{A}_{p_2}(i)$ is the i-th block of the AR parameters in (5) and of size $(p_2 + 1) \times (p_2 + 1)$.

The backward linear vector extrapolation is given by

$$\hat{\mathbf{s}}_{p_2}^B(n_1 - p_1, n_2) = -\sum_{i=1}^{p_1} (\mathbf{J}_{p_2} \mathbf{A}_{p_2}(i)^* \mathbf{J}_{p_2}) \mathbf{s}_{p_2}(n_1 - p_1 + i, n_2) \quad , \tag{6}$$

where * represents the conjugate operation. $\mathbf{J}_{p_2}$ is a reflection matrix of dimension $(p_2 + 1) \times (p_2 + 1)$ whose anti-diagonal elements are one and all other elements are zero, i.e.,

$$\mathbf{J}_{p_2} = \begin{bmatrix} 0 & 0 & \cdots & 1 \\ 0 & 0 & \cdots & \vdots \\ 0 & 1 & \cdots & 0 \\ 1 & 0 & \cdots & 0 \end{bmatrix} . \tag{7}$$

For more details about vector extrapolation equations, please see [7] and [11].

Therefore, the matrix $\mathbf{S}$ can be extrapolated to the matrix $\mathbf{S_E}$ as follows:

$$\mathbf{S_E} = \begin{bmatrix} \mathbf{S_U} \\ \mathbf{S} \\ \mathbf{S_D} \end{bmatrix} = \begin{bmatrix} g_1(0) & g_1(1) & \cdots & g_1(N-1) \\ g_2(0) & g_2(1) & \cdots & g_2(N-1) \\ \vdots & \vdots & \ddots & \vdots \\ g_{\alpha L}(0) & g_{\alpha L}(1) & \cdots & g_{\alpha L}(N-1) \end{bmatrix} , \tag{8}$$

where $\mathbf{S} = \begin{bmatrix} s_1(0) & s_1(1) & \cdots & s_1(N-1) \\ s_2(0) & s_2(1) & \vdots & s_2(N-1) \\ \vdots & \vdots & \ddots & \vdots \\ s_L(0) & s_L(1) & \cdots & s_L(N-1) \end{bmatrix} = \begin{bmatrix} g_{(\alpha-1)L/2+1}(0) & g_{(\alpha-1)L/2+1}(1) & \cdots & g_{(\alpha-1)L/2+1}(N-1) \\ g_{(\alpha-1)L/2+2}(0) & g_{(\alpha-1)L/2+1}(1) & \cdots & g_{(\alpha-1)L/2+2}(N-1) \\ \vdots & \vdots & \ddots & \vdots \\ g_{(\alpha+1)L/2}(0) & g_{(\alpha+1)L/2}(1) & \cdots & g_{(\alpha+1)L/2}(N-1) \end{bmatrix} . \alpha$

is the spatial extrapolation factor of the array. The original data set $\mathbf{S}$ is the central part of $\mathbf{S}_E$. $\mathbf{S_U}$ and $\mathbf{S_D}$ are extended data from the top and bottom of the matrix $\mathbf{S}$ respectively.

B. TR imaging based on SF-DORT

After having obtained the extrapolated data $\mathbf{S}_E$, the SF-MDM $\mathbf{K}$ can be established by applying Fourier transform to each row of $\mathbf{S}_E$. The matrix $\mathbf{K}$ has size $\alpha L \times N$ and can be expressed as below

$$\mathbf{K} = \begin{bmatrix} k_1(\omega_1) & k_1(\omega_2) & \cdots & k_1(\omega_N) \\ k_2(\omega_1) & k_2(\omega_2) & \vdots & k_2(\omega_N) \\ \vdots & \vdots & \ddots & \vdots \\ k_{\alpha L}(\omega_1) & k_{\alpha L}(\omega_2) & \cdots & k_{\alpha L}(\omega_N) \end{bmatrix} . \tag{9}$$

Appling SVD to $\mathbf{K}$, we have

$$\mathbf{K} = \mathbf{U}\mathbf{\Lambda}\mathbf{V} \tag{10}$$

where $\mathbf{\Lambda}$ is a $N \times M$ real diagonal matrix which contains singular values. $\mathbf{U}$ is an $N \times N$ unitary matrix, and $\mathbf{V}$ is the $M \times M$ matrix. Since the matrix $\mathbf{K}$ includes the spatial and frequency of the target, applying SVD to $\mathbf{K}$ is called SF decomposition. Assume $\mathbf{U}_p$ as the p-th column of the matrix $\mathbf{U}$, $\mathbf{V}_p$ as the p-th column of the matrix $\mathbf{V}$, and λ_p as the p-th singular value. $\mathbf{U}_p$ contains the spatial relationships between the p-th target and the extrapolated array while $\mathbf{V}_p$ represents the frequency content of the received signals. Assuming $S(\omega)$ as the Fourier transform of the transmitted signal $s(t)$, a new $N \times 1$ retransmitted vector function can be defined as below

$$\mathbf{R}_{\text{TR}}(\omega) = \mathbf{U}_p S(\omega) = \begin{bmatrix} U_{p,1} S(\omega) & U_{p,2} S(\omega) & \cdots & U_{p,\alpha L} S(\omega) \end{bmatrix}^{\text{T}} , \tag{11}$$

where $\mathbf{U}_p = \begin{bmatrix} U_{p,1} & U_{p,2} & \cdots & U_{p,\alpha L} \end{bmatrix}^{\text{T}}$ and "T" denotes transposition. By applying inverse Fourier transform to each row of $\mathbf{R}_{\text{TR}}(\omega)$, we could get the time-domain TR signal $\mathbf{r}_{\text{TR}}(t)$.

Once the vector $\mathbf{R}_{\text{TR}}(\omega)$ or $\mathbf{r}_{\text{TR}}(t)$ is obtained, we can get the following pseudo-spectrum $\mathbf{I}(\mathbf{P}_s)$ at the search point $\mathbf{P}_S$ in the spatial domain.

$$\mathbf{I}(\mathbf{P}_s) = \langle \mathbf{g}(\mathbf{P}_s, t), \mathbf{r}_{\text{TR}}(t) \rangle \big|_{t=0} = \int_\Omega \mathbf{G}(\mathbf{P}_s, \omega) \mathbf{R}_{\text{TR}}(\omega) d\omega , \tag{12}$$

where $\mathbf{G}(\mathbf{P}_s, \omega)$ is the Fourier transform of $\mathbf{g}(\mathbf{P}_s, t)$. $\Omega = \omega_N - \omega_1$. $\mathbf{G}(\mathbf{P}_s, \omega)$ is the background Green's function vector at the search point $\mathbf{P}_S = (x, y)$ to focus the target and is given by

$$\mathbf{G}(\mathbf{P}_s, \omega) = \begin{bmatrix} G(\mathbf{P}_s, \mathbf{R}_1, \omega) & G(\mathbf{P}_s, \mathbf{R}_2, \omega) & \cdots & G(\mathbf{P}_s, \mathbf{R}_N, \omega) \end{bmatrix}^{\text{T}} \tag{13}$$

with $G(\mathbf{P}_s, \mathbf{R}_1, \omega)$ is the background Green's function in free space, and $\mathbf{R}_n (n = 1, 2, \cdots, N)$ is the locations of the n-th antenna.

III. SIMULATIONS

In this section, we compare the range and co-range resolutions utilizing conventional SF-DORT and the proposed EA-SF-DORT for two different cases. The first is a single target case while the second is the multi-target one. We utilize SF-DORT to evaluate the targets detection performance.

The linear TR array is shown in Fig. 3. It contains 4 real antennas and 12 virtual antennas, so *L*=4 and the extrapolation factor *α*=4. All the antennas lie parallel to the x-axis. The distance between the adjacent antennas is set as *d* and *d* is 0.075m. The four real antennas are located at (50m, 0.25m), (50.075m, 0.25m), (50.15m, 0.25m) and (50.225m, 0.25m) respectively. The twelve virtual antennas

are located at (49.55m, 0.25m), (49.625m, 0.25m), (49.7m, 0.25m), (49.775m, 0.25m), (49.85m, 0.25m), (49.925m, 0.25m) and (50.3m, 0.25m), (50.375m, 0.25m), (50.45m, 0.25m), (50.525m, 0.25m), (50.6m, 0.25m), (50.675m, 0.25m) respectively.

The received LFM signal can be expressed in (2). The parameters of the LFM signal are as follows: B=0.5GHz, N=4000, $f_s = 4.5$GHz, $f_0 = 2.25$GHz. The signal to noise ratio (SNR) is 10 dB.
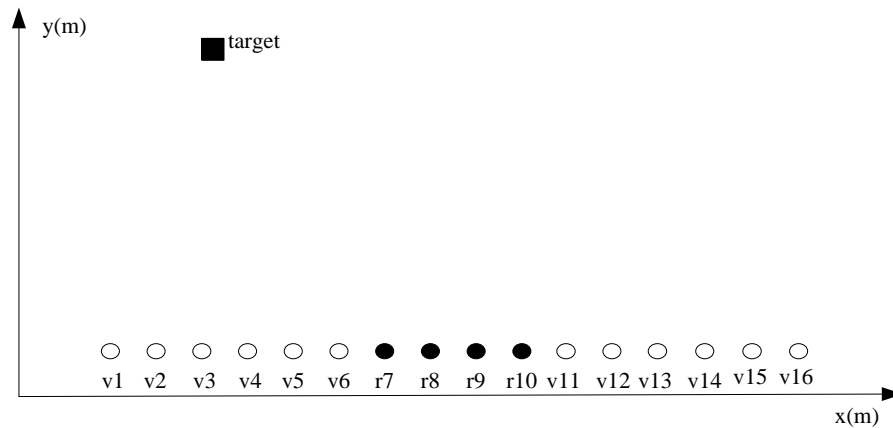

Fig. 3. Ilustration of the TR array placed parallel to the x-axis and the target in the far field, "v" denotes virtual antennas and "r" denotes real antennas.

A. Imaging for a single target case

Consider the single point target located at (62.5m, 75m). All the antennas in the TR array receives LFM signal.

The range and co-range resolutions given by SF-DORT with and without autoregressive vector extrapolation are shown in Fig 4. It can be observed that the peak appear at the target location with and without extrapolation, but the sidelobes are much lower and the mainlobe is much narrower when extrapolation is used. The raising in co-range resolution is superior to the raising in range resolution because the co-range resolution is inversely proportional to the effective aperture of the array and the proposed extrapolation method increases the aperture effectively.
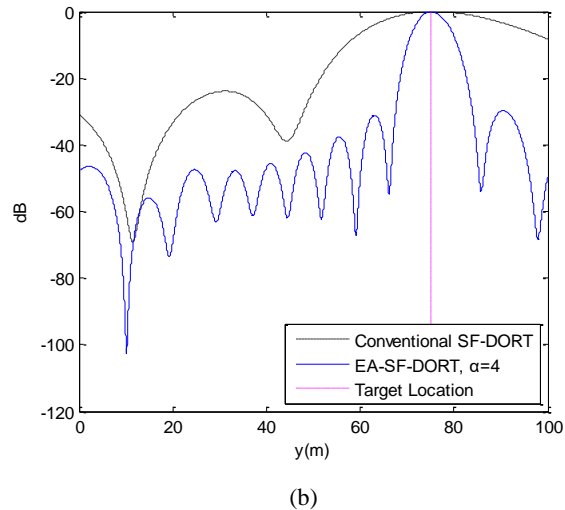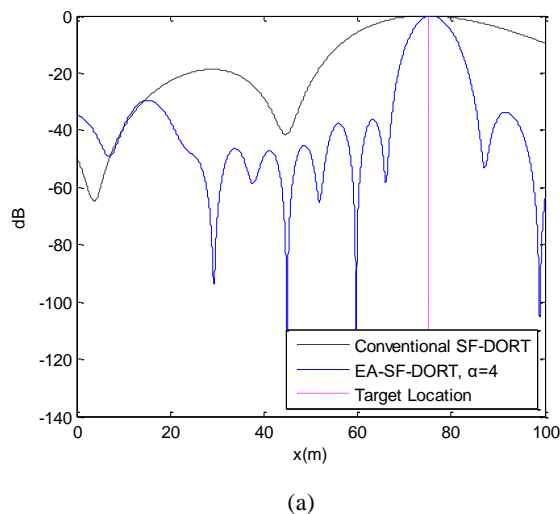

(a)

(b)
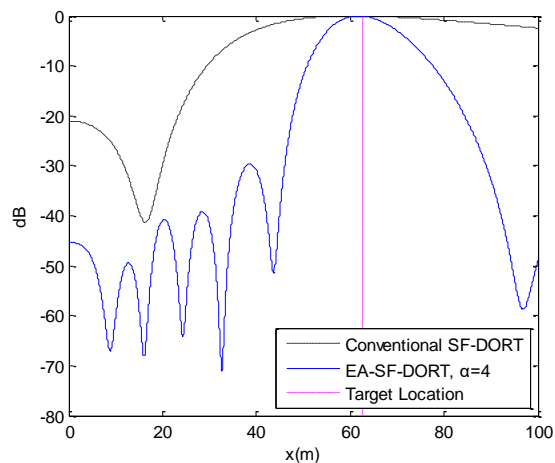
Fig. 4. Range and co-range resolutions utilizing SF-DORT and EA-SF-DORT for a single target and the target is located at (62.5m,75m) (a) Co-range resolutions (b) Range resolutions

B. Imaging for a multi-target case

In this simulation, we consider a two targets case when the targets are located at (75m,62.5m) and (25m, 37.5m) respectively. All the antennas in the TR array receive the same LFM signal. The extrapolation factor α is 4 and the extrapolated matrix $\mathbf{S}_E$ has the size of (16×4000). Once the left singular vectors $\mathbf{U}_p$, $p = 1, \ldots, P$, $P = 2$ have been acquired using (10), we could locate the two targets with the same procedure above.

The comparison of range and co-range resolutions for the target located at (75m, 62.5m) given by SF-DORT with and without ARVE are shown in Fig. 5, while the same comparison for the target located at (25m, 37.5m) are shown in Fig. 6. From Fig. 5 and Fig. 6 the range and co-range resolutions are much higher when extrapolation is used, especially the range resolution for the target at (25m, 37.5m).
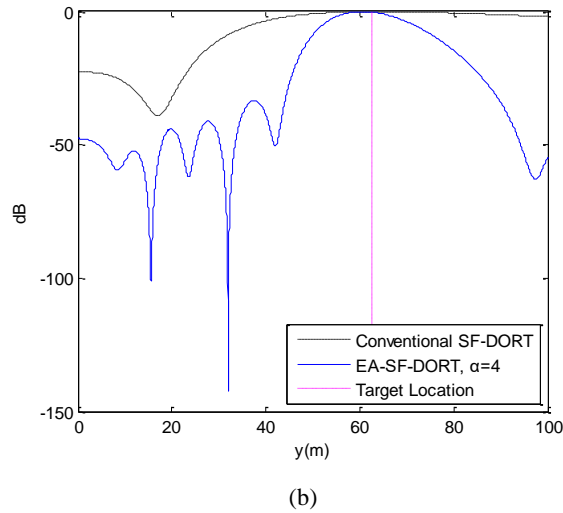

(a)

(b)

Fig. 5. Range and co-range resolutions utilizing SF-DORT and EA-SF-DORT for Multitargets case, the target is located at (75m,62.5m). (a) Co-range resolutions (b) Range resolutions
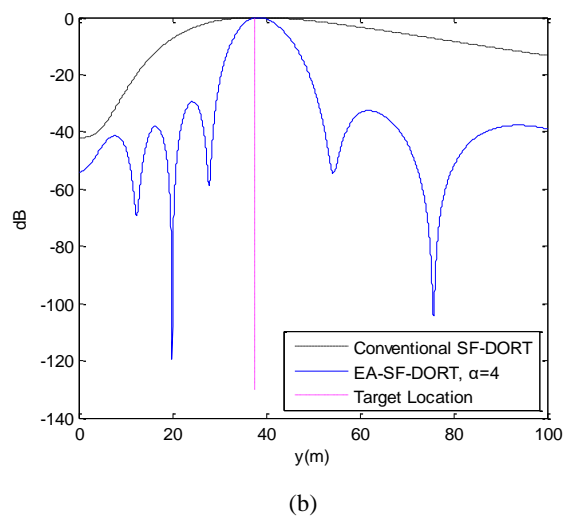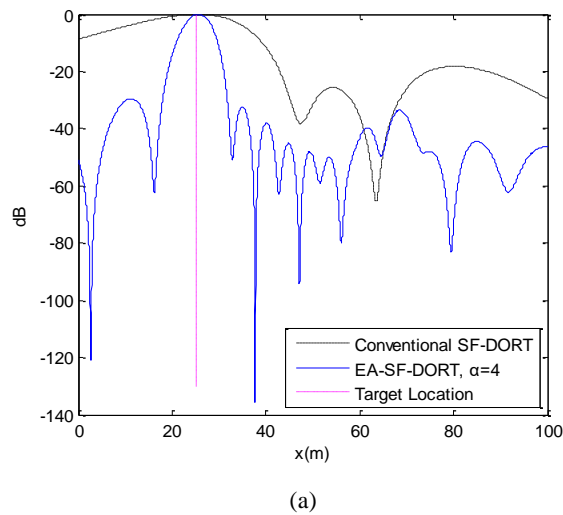

(a)

(b)

Fig. 6. Range and co-range resolutions utilizing SF-DORT and EA-SF-DORT for Multitargets case, the target is located at (25m,37.5m). (a) Co-range resolutions (b) Range resolutions

IV. CONCLUSION

In this paper, we have presented a novel high-resolution TR imaging method utilizing SF-DORT combining virtual array created by ARVE (EA-SF-DORT). The ARVE extends the aperture of the TR array significantly, consequently overcomes the shortcomings of conventional SF-DORT. It has been shown that the SF-DORT utilizing extrapolated virtual array achieves much higher range and co-range resolutions than conventional SF-DORT. Simulation results validate the satisfying performance of the proposed method.

ACKNOWLEDGMENT

REFERENCES

[1] Mathias Fink and Claire Prada. "Acoustic time-reversal mirrors", *Inverse Probl.*,Vol.17, No.3, pp. R1-R38, Feb. 2001. DOI: 10.1088/0266-5611/17/1/201.

[2] G. Micolau, M. Saillard. "D.O.R.T. method as applied to electromagnetic subsurface sensing", *Radio Sci.*, vol. 38,no. 3, pp. 4-1 - 4-12, Jun. 2003. DOI: 10.1029/2000RS002590.

[3] Mehmet E. Yavuz, Fernando L. Teixeira. "Full time-domain DORT for ultrawideband electromagnetic fields in dispersive, random inhomogeneous media", *IEEE Trans. Antennas Propag.*, vol. 54, no. 8, pp. 2305-2315, Aug. 2006. DOI: 10.1109/TAP.2006.879196.

[4] X.M. Zhong, C. Liao, W.B. Lin, H.Y. Li and H.J. Zhou. "Time-reversal imaging based on the space-frequency MDM and cancellation operator", *J. Electromagn. Waves Appl. s*,Vol.28, No.3, pp. 265-274, Feb. 2014. DOI: 10.1080/09205071.2013.861751

[5] Xuanming Zhong, Cheng Liao, and Wenbin Lin. "Space-Frequency Decomposition and Time-Reversal Imaging", *IEEE Trans. Antennas Propag.*,Vol.63, No.12, pp. 5619-5628, Dec. 2015. DOI: 10.1109/TAP.2015.2490579.

[6] Xuanming Zhong, Cheng Liao, and JuFeng. "Time-reversal time-domain imaging algorithm based on space-frequency decomposition", *Chin. J. Radio Sci.*,Vol.29, No.3, pp. 476-479, Jun. 2014.

[7] Mehmet E. Yavuz, Fernando L. Teixeira. "Space–Frequency Ultrawideband Time-Reversal Imaging", *IEEE Trans. Geosci. Remote Sens.*, vol. 46, no. 4, pp. 1115-1124, Mar. 2008. DOI: 10.1109/TGRS.2008.915755.

[8] M. E. Yavuz, A. E. Fouda, and F. L. Teixeira. "GPR Signal Enhancement Using Sliding-Window Space-Frequency Matrices", *Prog. Electromagn. Res.*, vol. 45, no. 4, pp. 1-10, 2014.

[9] Javad Ebrahimi-Zadeh, Mojtaba Dehmollaian, and Karim Mohammadpour-Aghdam. "Electromagnetic Time-Reversal Imaging of Pinholes in Pipes", *IEEE Trans. Antennas Propag.*, Vol.64, No.4, pp.1356-1363, Apr. 2016. DOI: 10.1109/TAP.2016.2526043.

[10] C. S. Marino and P. M. Chau. "Constrained Sensor System Resolves Closely Spaced Obscured Low-SNR Sources Using Virtual Beamforming", *IEEE Trans. Instrum. Meas.*, vol. 63, no. 1, pp. 231-242, Jan 2014. DOI: 10.1109/TIM.2013.2275239.

[11] C. S. Marino and P. M. Chau, "Low-Level Sinusoidal Signal Detection From a High-Resolution Virtual Spectral Image Using Autoregressive Vector Extrapolation," *IEEE Trans. Instrum. Meas.*, vol. 61, no. 9,pp. 2413–2421, Sep. 2012. DOI: 10.1109/TIM.2012.2190549.

[12] F. Wan, W.-P. Zhu, and M. N. S. Swamy, "Spacial Extrapolation-Based Blind DOA Estimation Approach for Closely Spaced Sources", *IEEE Trans.Aerosp. Electron. Syst.*, vol. 46, no. 2, pp. 569–582, Apr. 2010. DOI: 10.1109/TAES.2010.5461642.

[13] C. S. Marino and P. M. Chau : "High resolution full aperture processing of data limited scenarios through synthetically extending the temporal data", *Proc. 39th Asilomar Conf. on Signals, Syst. Comput.*, Pacific Grove, CA, USA, 2005, pp.1394-1398.

[14] S. L. Marple, Jr., *Digital Spectral Analysis*. Englewood Cliffs, NJ, USA: Prentice-Hall, 1987.

[15] B. Aksasse, L. Radouane, "Two-dimensional autoregressive(2-D AR) model order estimation", *IEEE Trans. Signal Process.*, vol. 47,no. 7, pp. 2072–2077, Jul. 1999. DOI: 10.1109/78.771063.